



저작자표시-비영리-변경금지 2.0 대한민국

이용자는 아래의 조건을 따르는 경우에 한하여 자유롭게

- 이 저작물을 복제, 배포, 전송, 전시, 공연 및 방송할 수 있습니다.

다음과 같은 조건을 따라야 합니다:



저작자표시. 귀하는 원저작자를 표시하여야 합니다.



비영리. 귀하는 이 저작물을 영리 목적으로 이용할 수 없습니다.



변경금지. 귀하는 이 저작물을 개작, 변형 또는 가공할 수 없습니다.

- 귀하는, 이 저작물의 재이용이나 배포의 경우, 이 저작물에 적용된 이용허락조건을 명확하게 나타내어야 합니다.
- 저작권자로부터 별도의 허가를 받으면 이러한 조건들은 적용되지 않습니다.

저작권법에 따른 이용자의 권리는 위의 내용에 의하여 영향을 받지 않습니다.

이것은 [이용허락규약\(Legal Code\)](#)을 이해하기 쉽게 요약한 것입니다.

[Disclaimer](#)

Master's Thesis
석사학위논문

Deep Neural Networks for Assessing Functional Connectivity: an fNIRS Study

Bahareh Behboodi (버하레)

Department of Information and Communication Engineering

정보통신융합공학전공

DGIST

2017

Master's Thesis
석사학위논문

Deep Neural Networks for Assessing Functional Connectivity: an fNIRS Study

Bahareh Behboodi (버하레)

Department of Information and Communication Engineering

정보통신융합공학전공

DGIST

2017

Deep Neural Networks for Assessing Functional Connectivity: an fNIRS Study

Advisor: Prof. Ji-Woong Choi
Co-advisor: Prof. Hyeon-Ae Jeon

by

Bahareh Behboodi
Department of Information and Communication Engineering
DGIST

A thesis submitted to the faculty of DGIST in partial fulfillment of the requirements for the degree of Master of Science in the Department of Information and Communication Engineering. The study was conducted in accordance with Code of Research Ethic¹.

December 29, 2017

Approved by

Professor Ji-Woong Choi _____
(Advisor)

Professor Hyeon-Ae Jeon _____
(Co-advisor)

¹ Declaration of Ethical Conduct in Research: I, as a graduate student of DGIST, hereby declare that I have not committed any act that may damage the credibility of my research. These include, but are not limited to: falsification, thesis written by someone else, distortion of research findings or plagiarism. I affirm that my thesis contains honest conclusions based on my own careful research under the guidance of my thesis advisor.

Deep Neural Networks for Assessing Functional Connectivity: an fNIRS Study

Bahareh Behboodi

Accepted in partial fulfillment of the requirements for the degree of Master of Science.

December 29, 2017

Head of Committee _____ (signature)

Prof. Ji-Woong Choi

Committee Member _____ (signature)

Prof. Hyeon-Ae Jeon

Committee Member _____ (signature)

Prof. Jae-Youn Hwang

MS/IC
201622001

버하레, Bahareh Behboodi. Deep Neural Networks for Assessing Functional Connectivity: an fNIRS Study. Department of Information and Communication Engineering. 2017. 33+iii pages. Advisor Prof. Ji-Woong Choi and Co-advisor Prof. Hyeon-Ae Jeon.

Abstract

Studies on interactions between brain regions estimate functional connectivity which are usually based on the basis of temporal presence. Functional connectivity derived from resting-state has been attracted by several recent studies as it provides valuable insight into the intrinsic networks of the human brain. Functional near-infrared spectroscopy (fNIRS) has gained attention in resting-state functional connectivity (RSFC) patterns detection because of its advantages compared to other neuroimaging modalities. Several progressive methodologies in detecting RSFC patterns in fNIRS, such as seed-based correlation analysis, and independent component analysis (ICA), were adopted in previous studies. Despite the fact that it is not known which methodology is the most suitable in detecting RSFC patterns, seed-based correlation analysis and ICA-based analysis which are the most widely used methodologies in RSFC studies, have intrinsic disadvantages. Therefore, in this study a method based on artificial neural network (ANN) was introduced to meet the possibilities of overcoming the conventional methods challenges. The RSFC patterns of the sensorimotor system derived from ANN were consistent with the previous findings. Moreover, the results of ANN illustrated the superior performance in the terms of specificity and sensitivity compared to both conventional approaches. The main contribution of the present thesis is to emphasize that ANN can be used as an appropriate method to estimate the temporal relation among brain networks during resting-state.

Keywords: Functional near-infrared spectroscopy, Functional connectivity, Seed-based correlation analysis, Independent component analysis, Artificial neural network.

Contents

Contents	i
List of Tables	ii
List of Figures	iii
I. INTRODUCTION	1
II. BASIC CONCEPTS AND BACKGROUND	4
1. Functional Near-Infrared Spectroscopy (fNIRS)	4
2. Discrete Wavelet Transformation as Band-pass Filter	4
3. Seed-based Correlation Analysis using General Linear Model (GLM)	5
4. Independent Component Analysis (ICA)	7
5. Artificial Neural Network (ANN)	7
6. Receiver Operating Characteristic (ROC) Curve	11
III. METHOD	12
1. Experimental Protocol	12
2. Concentration Changes of Hemoglobin	13
3. RSFC Estimation Using Seed-based Correlation Analysis	14
4. RSFC Estimation Using ICA	16
5. RSFC Estimation Using Artificial Neural Networks	17
6. Performance Evaluation Using ROC Curve	18
IV. RESULTS	20
1. Seed-based Correlation RSFC Results	21
2. ICA RSFC Results	22
3. ANN RSFC Results	22
4. ROC Evaluation Results	24
V. Discussion and Conclusion	26
References	28
Acknowledgments	32
Curriculum Vitae	33

List of Tables

3.1	Structure of ANN	18
------------	----------------------------	----

List of Figures

1.1	Hemodynamic response	2
2.1	Block diagram of ICA	8
2.2	Artificial neural network structure	8
2.3	Adam optimization algorithm	10
3.1	Task design of experiment	13
3.2	fNIRS optode configuration	13
3.3	Frequency range of detailed coefficients from 10 level wavelet decomposition .	14
3.4	Frequency range of wavelet detailed coefficients	15
3.5	Estimated Mixing Matrix and ICs from ICA	16
3.6	Selected Golden Standard for Performance Evaluation	18
4.1	Oxy-hemoglobin Fluctuations during Resting State	20
4.2	Results from Seed-based Correlation RSFC Analysis	21
4.3	Results from ICA RSFC Analysis	23
4.4	Results from ANN RSFC Analysis	24
4.5	Performance Evaluation Using ROC Curve	24

I. INTRODUCTION

The human brain has been represented as a complex system with intrinsic structurally and functionally interconnected networks. Statistical dependencies and synchronization of neurophysiological events of remote functional brain networks have been defined as brain functional connectivity [1]. Connectivity maps provide valuable insights into anatomical-functional architectures of the brain which can be measured not only during cognitive or motor tasks, but also during resting states. Resting state functional connectivity (RSFC) is the synchronization of spatially remote spontaneous brain activations which represents the interactions between neuronal activations while the brain is in its resting level. In the resting state, subjects are not required to perform any tasks so the brain is not simulated with any external stimulations. Researchers recently has focused on connectivity maps derived from brain networks as it showed potential for diagnosis of brain diseases [2–4]. For example, detection of abnormal functional connectivity has been used in characterizing patients with autism spectrum disorder [5], affective disorders [6], and depression [7]. Modern non-invasive neuroimaging modalities such as functional magnetic resonance (fMRI), electroencephalography (EEG), functional near-infrared spectroscopy (fNIRS), and megnetoencephalography (MEG) has shown an important role in exploring functional connectivity of the brain networks in both task and resting states of normal and patients with brain diseases.

Among all aforementioned modalities, functional near-infrared spectroscopy (fNIRS) as a promising tool for brain signal acquisition, offers high temporal resolution, long period of continuous data acquisition, and low burden on the participants. Several previous studies have presented the feasibility of using fNIRS in detecting resting-state functional connectivity using fNIRS [8–10]. fNIRS monitors hemodynamic response based on the change of hemoglobin level during brain activation by transmitting the near-infrared light (600~900 nm) through a path from transmitter, scalp, tissue, skull, brain, and receiver. The change of hemoglobin is caused by neurovascular coupling in the cerebral cortex. Therefore, the increase of oxygenated hemoglobin (HbO) and decrease of deoxygenated hemoglobin (HbR) can be utilized as a metric

for estimating brain activation. Oxy- and deoxy-hemoglobin absorb the light with different coefficients (see Fig. 1.1). Eventually, the difference of the light intensity in fNIRS's sources and detectors can be converted to the oxy- and deoxy-hemoglobin level using Beer-Lambert law [11, 12]. Chapter II provides more details on principles of fNIRS.

Numerous connectivity analyses have been explored in all aforementioned neuroimaging modalities in order to identify inter-connected brain networks. They usually entail finding predominant patterns based on statistical dependencies measurements. The most common analysis methods in fNIRS are seed-based correlation analysis [9] and independent component analysis (ICA) [13] in which each of them models latent factors from data by considering a linear-mixing problem of the input data [11]. In seed-based correlation analysis, seed-regions should be determined as the region of interest (ROI). After the selection of ROI (seed), temporal correlations of selected ROI with all other channels are computed and the resting-state functional connectivity (RSFC) maps from the fNIRS data acquired during a resting state, can be constructed [9]. In ICA-based analysis of RSFC, data from whole channels of a resting state is divided into several statistically independent components including RSFC networks [13] (chapter II will provide more details). Although, the two above mentioned methods have several inherent problems [13–15], it is not known which method can best describe the intrinsic networks. To date, studies on estimating RSFC maps based on fNIRS are in their early stages and there is

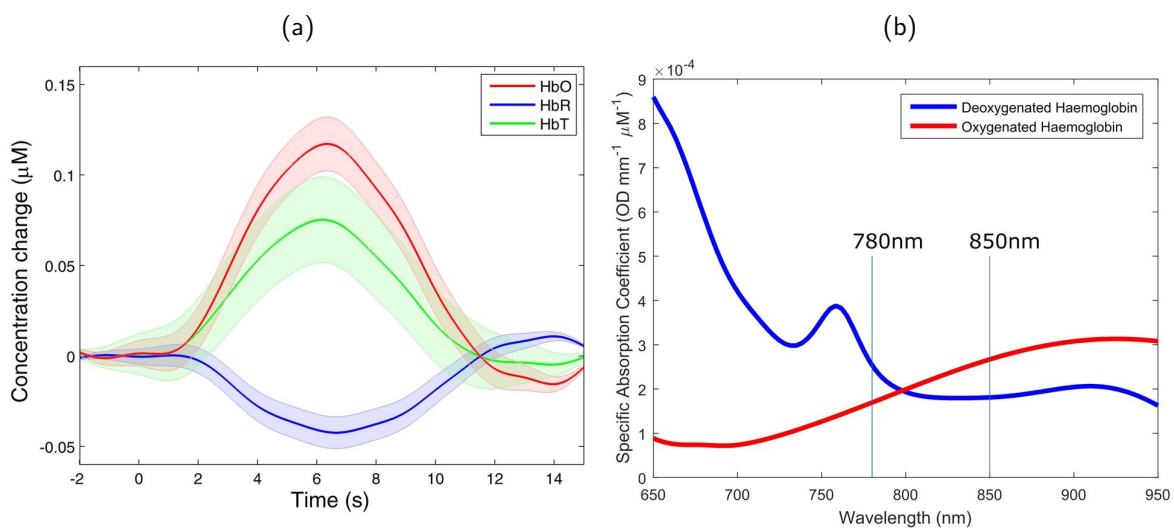


Figure 1.1. Physiological response of hemodynamic signal. (a) Concentration changes of HbO, HbR, and total hemoglobin represented (HbT) are presented in red, blue, and green lines, respectively. Stimulus period is presented at 0 second. (b) Light absorption differences in Oxy- (red) and Deoxy-hemoglobin (blue).

no unified standard for analyzing resting-state fNIRS data [8].

Recent new machine learning algorithms has brought a wide applications in signal and image analysis [16–18]. Artificial neural networks (ANN) have some distinguishing aspects that make them attractive. They are data-driven, nonlinear methods which are able to generate an appropriate mapping between their inputs and outputs [19]. Thereby, it is reasonable that neural networks may be able to enhance the performance in constructing connectivity networks. In this thesis, a deep artificial neural network has been utilized to construct functional connectivity maps from fNIRS signals while measured during a resting-state. Eventually, the performance of RSFC maps derived from neural networks have been compared with the aforementioned conventional schemes in constructing connectivity maps.

The chapters of this thesis are separated into five parts: introduction in chapter I, basic concepts and background in chapter II, method in chapter III, results in chapter IV followed by discussion and conclusion in chapter V. Chapter II includes the basic principles of fNIRS, conventional and proposed method in estimating RSFC maps. The experimental procedure, signal processing, and estimation of RSFC maps can be found in chapter III. Chapter IV presents the results obtained from the conventional and proposed schemes. The discussion and conclusion are given in chapter V.

II. BASIC CONCEPTS AND BACKGROUND

1. Functional Near-Infrared Spectroscopy (fNIRS)

As briefly mentioned in chapter I, fNIRS has been utilized as an emerging non-invasive brain imaging technique. fNIRS basically relies on the principles of the neuro-vascular coupling which is also known as hemodynamic response. Through neuro-vascular coupling, neuronal activity is followed by changes in localized blood flow including hemoglobin. The change in hemoglobin during neuronal activation leads the increase of oxygenated hemoglobin (HbO) and decrease in deoxygenated hemoglobin (HbR) as was shown of Fig. 1.1(a) in chapter I. Both HbO and HbR concentrations absorb the light intensity, though with different coefficients. This difference absorption coefficients can be used as a metric in estimating the changes of HbO and HbR concentration which is the principles of modified Beer-Lambert law (MBLL) [11,20]. The light intensity is transmitted from fNIRS transmitter and after passing through scalp, tissue, and skull, it is received in fNIRS receivers. The measured light intensities is converted into the concentration changes of HbO and HbR using MBLL. The MBLL equation is expressed by

$$\begin{bmatrix} \Delta[HbO] \\ \Delta[HbR] \end{bmatrix} = \frac{1}{d \cdot DPF} \begin{bmatrix} \epsilon_{\lambda_1}^{HbO} & \epsilon_{\lambda_1}^{HbR} \\ \epsilon_{\lambda_2}^{HbO} & \epsilon_{\lambda_2}^{HbR} \end{bmatrix}^{-1} \begin{bmatrix} \Delta OD_{\lambda_1} \\ \Delta OD_{\lambda_2} \end{bmatrix} \quad (2.1)$$

where the concentration changes of HbO and HbR are defined as $\Delta[HbO]$ and $\Delta[HbR]$, respectively. d is the distance between light source and detector. DPF is the differential path length factor. ϵ is the extinction coefficient at wavelength λ , and ΔOD is the light intensity change.

2. Discrete Wavelet Transformation as Band-pass Filter

fNIRS contains different types of noises. One of the filtering methods of the raw fNIRS data is based on discrete wavelet transformation. The discrete wavelet transform decomposes the signal, $S[n]$, into different coefficients named as approximation and detailed coefficients each with specific range of frequencies. The mentioned coefficients can be obtained by the

scaling function ($\phi_{j_0,k}[n]$) and wavelet function ($\psi_{j,k}[n]$) (j , and k are scaling and translating parameters, respectively. Please refer to [21] for more details.) through below equations;

$$A_\phi[j_0, k] = \frac{1}{\sqrt{M}} \sum_n S[n] \phi_{j_0,k}[n], \quad (2.2)$$

and

$$D_\psi[j, k] = \frac{1}{\sqrt{M}} \sum_n S[n] \psi_{j,k}[n], \quad (2.3)$$

where M is the total points, $A_\phi[j_0, k]$ is approximation coefficient, $D_\psi[j, k]$ is detailed coefficient. Then, a signal $S[n]$ can be expressed by

$$S[n] = \frac{1}{\sqrt{M}} \sum_k A_\phi[j_0, k] \phi_{j_0,k}[n] + \frac{1}{\sqrt{M}} \sum_{j=j_0}^{\infty} \sum_k D_\psi[j, k] \psi_{j,k}[n]. \quad (2.4)$$

The approximation coefficients and detailed coefficients can be rewritten as

$$a_{j_0} = \frac{1}{\sqrt{M}} \sum_k A_\phi[j_0, k] \phi_{j_0,k}[n], \quad (2.5)$$

and

$$d_j = \frac{1}{\sqrt{M}} \sum_k D_\psi[j, k] \psi_{j,k}[n], \quad (2.6)$$

so, the signal $S[n]$ can be reconstructed from the mentioned components by

$$S[n] = a_{j_0} + \sum_{j=-\infty}^{j_0} d_j. \quad (2.7)$$

Eventually, the signal can be reconstructed by picking the coefficients whose range of frequency is aligned with the desired cutoff frequency. The reconstructed signal represents the filtered signal [22].

3. Seed-based Correlation Analysis using General Linear Model (GLM)

Seed-based correlation analysis is one the most commonly used method in detecting functional connectivities. In the simplest seed-based functional connectivity, the correlation between the times-series of one fNIRS channel (known as seed) and all the other channels is exploited [23].

In order to calculate the correlations, general linear model (GLM) has been utilized in this thesis as explained in [9]. The standard linear model of brain activity can be expressed by

$$Y = X.\beta + \varepsilon, \quad (2.8)$$

where Y is a column vector of the oxy-hemoglobin time series from a channel. X is known as the design matrix. In the case of functional connectivity study in fNIRS, it includes the oxy-hemoglobin time points of the selected seed as a regressor in the linear model. The design matrix should additionally contain a constant column for modeling the mean of the signal. The variable β defines the unknowns which are going to be estimated by the given input data (Y) and the design matrix (X) in order to reduce the error represented as ε . In other words, the time points of fNIRS channel is modeled as the sum of weighted columns of the design matrix. To be more specific, GLM can model the time points of all the fNIRS channels (excluding selected channel as the seed) based on the time points of the selected seed and result in estimated β s. The linear regression model in Eq. 2.8, is typically solved using the least-squares method. Thereby, the best estimate of β can be derived by

$$\beta = (X^T.X)^{-1}.X^T.Y, \quad (2.9)$$

Next, statistical T -test can be used in order to test whether the estimated β s are nonzero or not by

$$T = c.\beta / \sqrt{c.(X^T.X)^{-1}.\sigma^2.c^T}, \quad (2.10)$$

where σ^2 is the mean-squared error of the residuals ($\sigma^2 = \langle \varepsilon^2 \rangle$) and c is the contrast vector. For example, to test if the second coefficient of the β vector is nonzero the contrast would be $c = [0 \ 1]$ in case of only having two regressors in the design matrix. Consequently, T -values are corresponded to the correlations of each channel with the selected seed which are known as connectivity maps [9, 23, 24].

4. Independent Component Analysis (ICA)

Independent component analysis (ICA) is one of the most widely used methods among blind source separation (BSS) techniques. In BSS one of the classic problems is known as the cocktail party problem. In this problem, there are several microphones in a conference hall which collect a mixture of individuals' spoken voices. It is of interest to separate each individual signal from the mixture signals. Solving this problem is the aim of BSS technique [25].

ICA assumes that the sources of individuals' voices are independent from each other. In the case of fNIRS, measured signals from fNIRS channels can be regarded as the mixture of the voices recorded by microphones in the cocktail party problem [13]. Suppose there are N channels which have been measured for T time points. The mixture signals can be represented by $x(t) = [x_1(t), x_2(t), \dots, x_N(t)]^T : (t = 1, 2, \dots, T)$. The independent sources $s(t) = [s_1(t), s_2(t), \dots, s_N(t)]^T : (t = 1, 2, \dots, T)$ can be derived using ICA by

$$x(t) = A.s(t), \quad (2.11)$$

where A is the mixing matrix. The sources $s_i(t)$ can be recovered from only the measured signals $x_i(t)$. Incidentally, the reason for describing this technique as *blind* is that there is no prior information about the mixing matrix and sources. The estimation of sources, $\hat{s}(t)$, is obtained by

$$\hat{s}(t) = W.x(t), \quad (2.12)$$

where $W^{-1} = \hat{A}$ is the un-mixing matrix in which \hat{A} represents the estimated mixing matrix. Figure 2.1 summarizes the procedure of ICA technique. In fNIRS, \hat{A} includes the RSFC maps which chapter. III presents more details.

5. Artificial Neural Network (ANN)

Artificial neural network (ANN) is a machine learning technique which can be used to perform nonlinear statistical modeling. It is basically inspired by the biological model of human brain, specifically the bioelectrical activity of the neurons in the brain. The interconnected neurons

of ANN, as they exchange information with each other, they can be a simplified simulations of how brain regions interact with each other. ANN has been utilized in various domains including business, engineering, and medicine. ANN offers a number of advantages, including requiring less formal statistical training, ability to implicitly detect complex nonlinear relationships and interactions in the data, and the availability of multiple training algorithms [17, 26, 27].

In general, ANN consists of several layers known as input layer, hidden layer(s), and output layer. Each layer contains one or more neurons (see Fi. 2.2) in which their values are updated through several forward and backward propagation of training process. Through

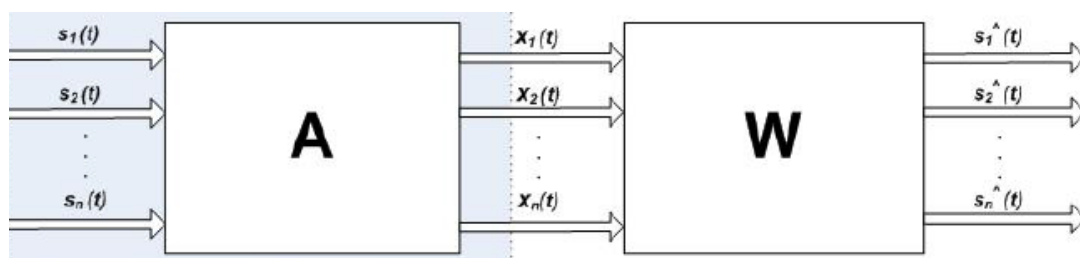


Figure 2.1. Independent component analysis (ICA) block diagram. $s(t)$, A , $x(t)$, W , $\hat{s}(t)$ are the sources, mixing matrix, measured signals, un-mixing matrix, and estimated signals by using ICA, respectively (adopted form [25]).

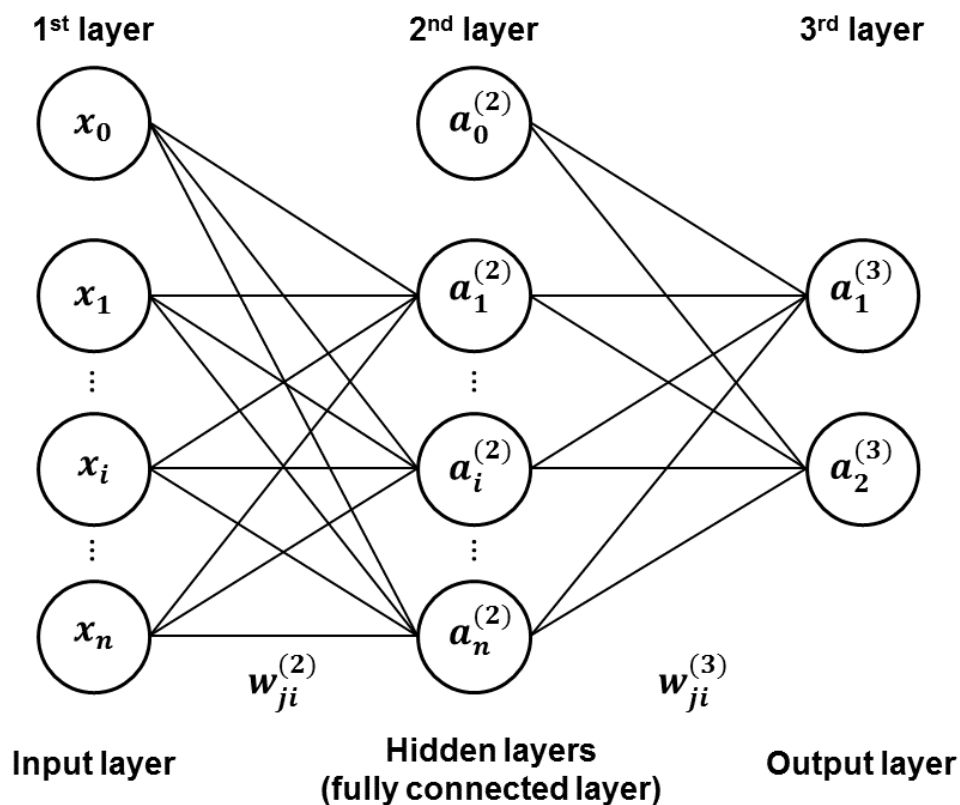


Figure 2.2. The structure of ANN consists of input layer, hidden layer(s), and output layer.

forward propagation, the values of neurons can be determined by

$$a_i^l = f\left(\sum_i w_{ji}^l a_j^{l-1}\right) \quad (2.13)$$

where a_j^l is defined as the output of the activation function $f(\cdot)$ in which its input is the output of j^{th} neuron of the l^{th} layer. w_{ji}^l is denoted as the weight for the connection from j^{th} neuron in the l^{th} layer, to the i^{th} neuron in the $(l-1)^{th}$ layer. a_0^l denotes the bias value. In case of computing values for the second layer, the Eq. 2.13 will be

$$a_i^2 = f\left(\sum_i w_{ji}^2 x_j\right) \quad (2.14)$$

Among various activation functions; i.e. $f(\cdot)$ in Eq. 2.13 and 2.14, here two of them are presented.

Rectifier Linear Unit (ReLU) activation function is an element-wise function which filters the negative inputs. In other words, it is off for the negative and on for the positive inputs. ReLU compared to other activation functions, has major benefit of converging to the optimum point much faster. Denoting $\sum_i w_{ji}^l a_j^{l-1}$ as z , this function is expressed by [28]

$$f(z) = \begin{cases} 0 & \text{if } z < 0 \\ z & \text{if } z \geq 0. \end{cases} \quad (2.15)$$

Softmax is another activation function which normalized a set of its input to the range of 0 and 1 such that each can be interpreted as the probability. The function is given by

$$f(z)_j = \frac{e^{z_j}}{\sum_i e^{z_i}} \quad (2.16)$$

Through training procedure weights and biases can be adopted in order to model the desired outputs. The training procedure can be repeated for several iterations of forward and backward propagation with respect to optimizing the loss function. In optimization problems, the loss function is a function from a set of variables or values [29]. ANN is typically trained using gradient based optimization methods. To be more specific, gradient descent finds a local minimum

of the loss function by taking steps proportional to the negative of the approximate gradient of the loss function at the current point. Eventually, gradient descent updates the parameters using the following rule,

$$\theta_{t+1} \leftarrow \theta_t - \eta \nabla_{\theta_t} L(x, \theta_t) \quad (2.17)$$

where η is called as the learning rate, θ is the parameter which need to be updated, and L represents the loss function. In recent years, several algorithms have been proposed instead of gradient descent. The Adam algorithms is one of the most efficient ways in updating parameters in which it adapts the learning rate of each parameter by scaling them [30]. In the current thesis, Adam optimization has been utilized. Figure 2.3 shows a schematic of the Adam algorithm.

ANN is basically a supervised learning method in which it is trained based on the given input data with its labels. The input data is separated to two groups, one for training and the other one for testing in order to evaluate its performance. However, in this thesis ANN has been used as a semi-supervised learning techniques. In semi-supervised algorithms, the labels are not given and they can be derived based on the input data. In the case of fNIRS, the ANN is trained based on the time series of resting-state of two selected channels and is tested on the remained channels (see chapter III for more details.)

Require: α : Stepsize
Require: $\beta_1, \beta_2 \in [0, 1)$: Exponential decay rates for the moment estimates
Require: $f(\theta)$: Stochastic objective function with parameters θ
Require: θ_0 : Initial parameter vector
 $m_0 \leftarrow 0$ (Initialize 1st moment vector)
 $v_0 \leftarrow 0$ (Initialize 2nd moment vector)
 $t \leftarrow 0$ (Initialize timestep)
while θ_t not converged **do**
 $t \leftarrow t + 1$
 $g_t \leftarrow \nabla_{\theta} f_t(\theta_{t-1})$ (Get gradients w.r.t. stochastic objective at timestep t)
 $m_t \leftarrow \beta_1 \cdot m_{t-1} + (1 - \beta_1) \cdot g_t$ (Update biased first moment estimate)
 $v_t \leftarrow \beta_2 \cdot v_{t-1} + (1 - \beta_2) \cdot g_t^2$ (Update biased second raw moment estimate)
 $\hat{m}_t \leftarrow m_t / (1 - \beta_1^t)$ (Compute bias-corrected first moment estimate)
 $\hat{v}_t \leftarrow v_t / (1 - \beta_2^t)$ (Compute bias-corrected second raw moment estimate)
 $\theta_t \leftarrow \theta_{t-1} - \alpha \cdot \hat{m}_t / (\sqrt{\hat{v}_t} + \epsilon)$ (Update parameters)
end while
return θ_t (Resulting parameters)

Figure 2.3. Adam learning algorithm [30].

6. Receiver Operating Characteristic (ROC) Curve

Receiver operating characteristic (ROC) curve is a fundamental tool for a test evaluation. It is a graphical plot which illustrates the performance of a test (in here a binary classifier system) compared to the golden standard of the results. In a ROC curve the true positive rate is plotted in the function of false positive rate based on different thresholds. Eventually, the area under the ROC curve (AUC) is the quantitative index for describing the performance [31]. The larger area under the curve represents better performance. In the case of fNIRS RSFC, the results of all aforementioned methods for estimating RSFC will be compared with a golden standard using ROC curve in chapter IV of this thesis.

III. METHOD

1. Experimental Protocol

The aim of this study is to investigate the resting state functional connectivity of Sensorimotor area. Therefore, a total of ten young adults (all right handed, mean age 22.8 ± 3.8 , four males) from DGIST University participated in this thesis project. None of the participants had history of motor or neurological disease or brain injury. All the participants were asked to avoid drinking alcohol or coffee in the day of experiment. Before the experiment, informed consent form was obtained according to the procedure approved by the DGIST Institutional Review Board (DGIST_170614-HR-010-02).

Participants underwent an experiment including two runs of fNIRS measurements. In the first run of the experiment, called as resting-state session, participants were asked to sit on a comfortable chair in a silent room with dim lighting. The participants were instructed to stay stable during the measurement with their eyes closed, remain motionless as much as possible, and try to relax their mind. Resting-state session lasted 8 minutes for each participant. Through second run, called as task session, participants were instructed to conduct bilateral finger tapping task which was shown in a laptop with 13-inch display monitor were placed approximately 80 cm in front of the participant. Task session included seven bilateral finger tapping blocks in which each of them lasted 28 seconds and followed by a 30 seconds fixation baseline. Through finger tapping blocks, fourteen random strings containing four characters were shown for 1.5 seconds followed by a 0.5 seconds fixation point. The characters in each string could be "L" or "R" representing right-hand or left-hand finger tapping, respectively (see figure 3.1).

During both runs, brain activation was measured using LABNIRS from Shimadzu with three wavelength (780, 805, and 830 nm) and sampling frequency of 18.51 Hz. 17 transmitters and 16 receivers leading 52 channels were placed on participant's head using a head cap which covers the whole brain, however, the fNIRS probes were set to only cover the Sensorimotor and Motor cortex following 10-20 international system. Figure 3.2 illustrates the channel

configuration.

2. Concentration Changes of Hemoglobin

The oxy-hemoglobin and deoxy-hemoglobin at each time point from each channel were computed using MBLL (see Eq. 2.1). As the data pre-processing for each aforementioned methods varies, in the following sections more details for each method will be presented. In this thesis only oxy-hemoglobin were considered for the data analysis. For simplicity, signal is used to refer to oxy-hemoglobin signal.

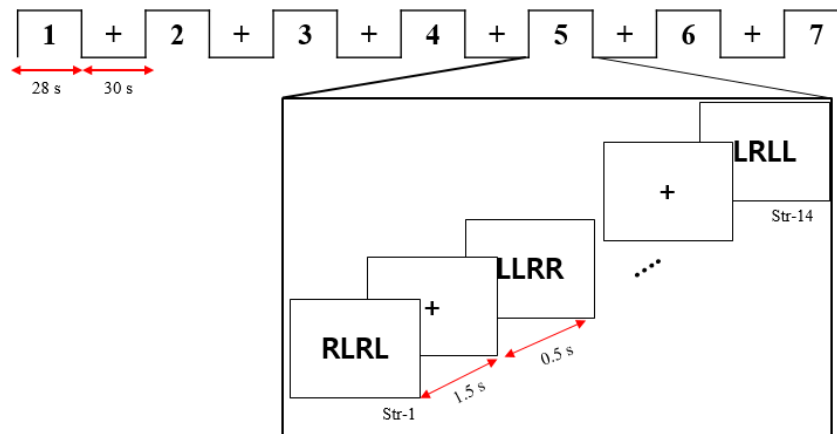


Figure 3.1. Task session includes seven finger tapping and six baseline blocks

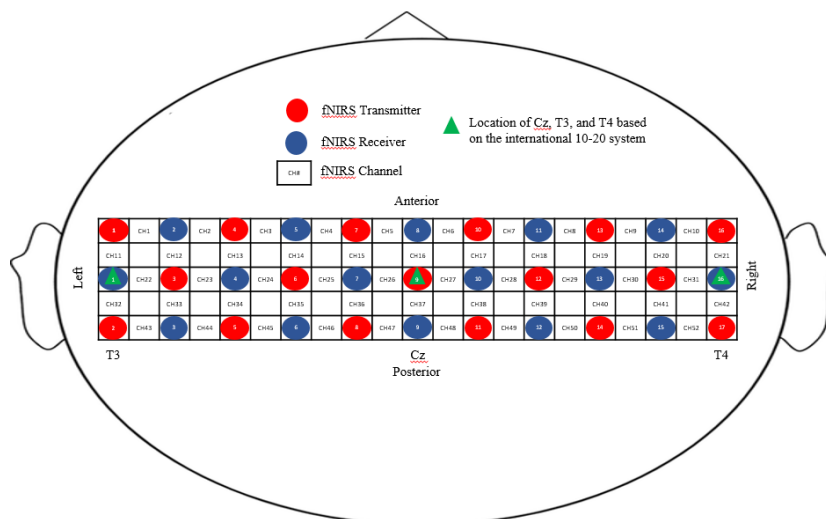


Figure 3.2. The configuration of fNIRS transmitters and receivers for an experiment

3. RSFC Estimation Using Seed-based Correlation Analysis

In the seed-based correlation analysis, first, the channel which was significantly stimulated during the task session, was selected as the seed. Next, individual RSFC estimation was performed using the seed time points in resting-state session. In the following paragraphs, it will be elaborated on the details of data processing for the seed-selection procedure followed by RSFC maps detection.

Before starting the measurement of task session, to make sure the signal reached its steady state, participants were asked to be ready and stay stable for 30 seconds. After data acquisition for task session and MBLL processing, to remove the high-frequency physiological noise and low-frequency baseline drift, a band-pass filter using discrete wavelet transformation was exploited as described in chapter II section 2. [22]. The desired high and low cutoff frequencies in fNIRS studies are $0.01 \sim 0.1$ Hz [20]. Figure 3.3 represents the physiological noises which are contaminated with hemodynamic response. A 10 level wavelet decomposition using Daubechies (db5) mother function was applied in order to remove undesired high and low frequency components of physiological noises. Therefore, the combination of detailed components d_8 and d_9 were selected to construct the filtered signal (in Eq. 2.7, $\tilde{S}[n] = d_8 + d_9$) as they contains the desire frequency range (see Fig.3.4).

Afterwards, GLM (see section 3. of chapter II) was used to infer which channel was statistically activated during the task session for each participant. The design matrix was obtained

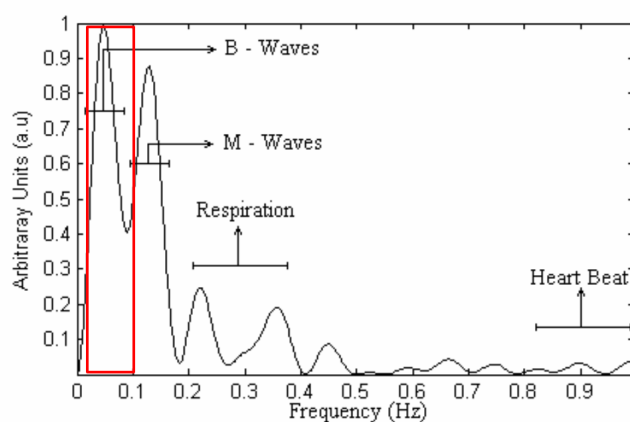


Figure 3.3. Physiological noises in fNIRS signal including heart rate, respiration, mayer wave (M-wave), and very low frequency oscillations (B-wave). The red square shows the desire frequency range ($0.01 \sim 0.1$ Hz) for hemodynamic response [20].

by the convolution of task onsets with canonical hemodynamic response function. Using the designed matrix, GLM was applied to the signal of each channel for all participants and yielded corresponding T -values. Therefore, individual activation T-maps were constructed based on 52 derived T -values [9, 32]. Thereafter, a group-level Wilcoxon Signed Rank test (known as summary statistics approach [33]) was performed on obtained T -values to find the most activated channel among all participants defined as the seed for the RSFC analysis. Wilcoxon Signed Rank is a non-parametric statistical hypothesis test to assess whether a distribution has a median equal to zero. It can be used as an alternative to the one-sample t -test. The results from Wilcoxon Signed-Rank are represented in the term of p -values. The lower p -value indicates

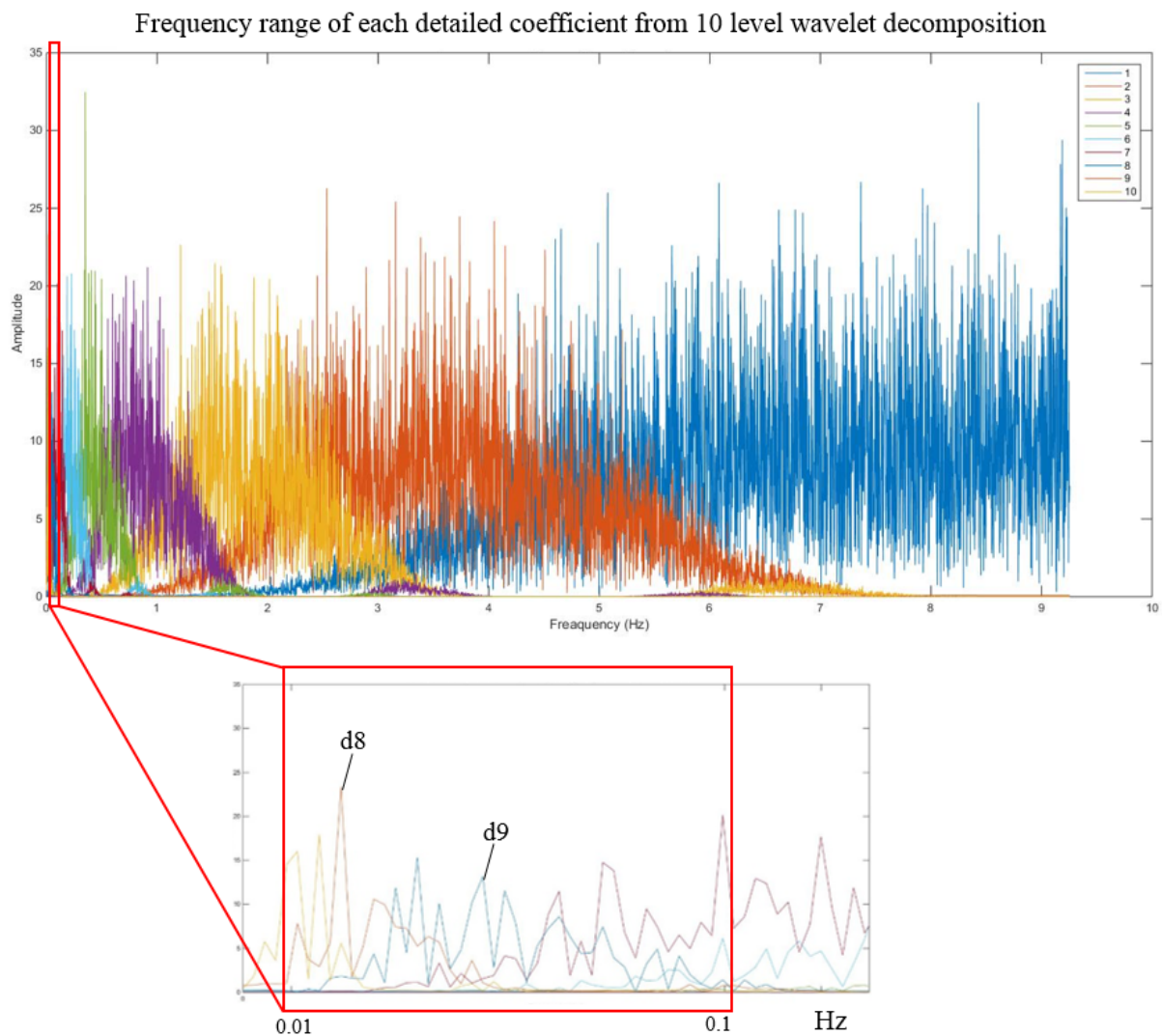


Figure 3.4. Each of detailed coefficients from 10 level wavelet decomposition has specific range of frequency in which $d8$ and $d9$ cover the desired frequency range of hemodynamic response. Each color represents the frequency range of a detailed coefficient.

higher significance.

The first 2 minutes of resting session data were discarded in order to reach the steady state. The filtered signals from resting session were extracted using wavelet transformation as explained above. The GLM was used similar to the above, however, the design matrix only included the resting data time points from the selected seed. Similarly, 52 T -values as the individual RSFC maps were derived for each participant. Next, group-level analysis using one-sample t -test was applied to identify channels that were significantly connected to the seed channel, defined as the group RSFC-map based on seed-correlation.

4. RSFC Estimation Using ICA

In this thesis, temporal ICA was exploited because of the large number of time points compared to relatively a small number of channels in fNIRS data [8, 13]. *FastICA* v2.5 was adopted to implement ICA analysis [34]. The parameters were chosen as discussed in [13]. For RSFC detection based on ICA only the data from resting session was considered. After MBLL analysis and excluding the first 2 minutes of the data, in order to filter the linear and bilinear trends from the remaining data, first and second order polynomial functions were adopted for de-trending the raw signals [35]. ICA was applied to 52 de-trended signals and yielded to 52 independent signals with a mixing matrix including the RSFC estimation.

To be more specific, let's consider $x(t)$, $\hat{s}(t)$, and \hat{A} as the fNIRS signal, estimated inde-

$$\begin{array}{c}
 \mathbf{x}(t) \text{ (oxy-hemoglobin signals for one subject)} \\
 \begin{array}{|c|c|c|c|c|}
 \hline
 \text{channel_1} & x(1,t_0) & x(1,t_1) & \dots & x(1,t_{\text{point}}) \\
 \hline
 \text{channel_2} & x(2,t_0) & x(2,t_1) & \dots & x(2,t_{\text{point}}) \\
 \hline
 \dots & \dots & \dots & \dots & \dots \\
 \hline
 \text{channel_52} & x(52,t_0) & x(52,t_1) & \dots & x(52,t_{\text{point}}) \\
 \hline
 \end{array} \\
 \\
 \hat{\mathbf{A}} \text{ (Mixing Matrix)} & \times & \hat{\mathbf{s}}(t) \text{ (Independent Components)} \\
 \begin{array}{|c|c|c|c|}
 \hline
 a(1,1) & a(1,2) & \dots & a(1,52) \\
 \hline
 a(2,1) & a(2,2) & \dots & a(2,52) \\
 \hline
 \dots & \dots & \dots & \dots \\
 \hline
 a(52,1) & a(52,2) & \dots & a(52,52) \\
 \hline
 \end{array} & & \begin{array}{|c|c|c|c|c|}
 \hline
 \text{Signal-1} & s(1,t_0) & s(1,t_1) & \dots & s(1,t_{\text{point}}) \\
 \hline
 \text{Signal-2} & s(2,t_0) & s(2,t_1) & \dots & s(2,t_{\text{point}}) \\
 \hline
 \dots & \dots & \dots & \dots & \dots \\
 \hline
 \text{Signal-52} & s(52,t_0) & s(52,t_1) & \dots & s(52,t_{\text{point}}) \\
 \hline
 \end{array} \\
 \\
 \end{array} =$$

Figure 3.5. Matrix dimensions of estimated independent components and mixing matrix derived from ICA.

pendent components, and estimated mixing matrix by ICA, respectively. The dimensions of the input and outputs of ICA can be shown in Fig. 3.5. The power spectrum of all the estimated independent components (e.g. signal-1, ..., signal-52 in Fig. 3.5) was obtained. The component of interest was selected if it had a prominent low frequency around the desire range of frequency for hemodynamic response; i.e. 0.01~0.1 Hz. The corresponding column of the selected component of interest in the mixing matrix represents the individual RSFC (e.g. if *Signal* – 2 was selected as the component of interest, $a(1,2)$, ..., $a(52,2)$ would represent the RSFC map). Next, individual RSFC maps were converted to standardized z -scores by

$$z_{ij} = \frac{a(i,j) - \mu}{\sigma} \quad (3.1)$$

where $a(i,j)$ is the ij th element of corresponding column from the mixing matrix. μ and σ are the mean and standard deviation of the selected column in the mixing matrix, respectively. Similar to RSFC estimation using GLM, group-level analysis was conducted on the individual RSFC z -scores using two-tailed one-sample t -test leading to group RSFC-map based on ICA analysis.

5. RSFC Estimation Using Artificial Neural Networks

Data pre-processing was applied to the resting state data similar to the section 3. of this chapter. Therefore, the filtered signals were passed through the ANN layers. In this thesis, a 4-layer ANN including input layer, 2 hidden layers, and an output layer was utilized. The details of the ANN structure is summarized in the table 3.1 (for more details of ANN please refer to chapter II, section 5.). In the input layer, number of neurons were equal to the number of time points of the resting-state data.

For training the ANN, two classes were defined. Based on the selected seed in RSFC estimation using GLM, ANN was trained considering the seed as the class (a). Channel 11 was chosen as the class (b) based on its anatomical location. For all the participants, ANN was trained for 20 trials containing 50 epochs in each. In the proposed structure of ANN, the activation function in input and hidden layers were set to ReLU. Adam optimizer was utilized in which the learning rate was set to 0.001. *Tensorflow* platform (<https://www.tensorflow.org/>)

based on NVIDIA GPU (GeForce GTX 1070) was used for ANN implementation. After training the ANN on all the participants, the mean of the channels' labels were computed in order to construct the group RSFC map.

6. Performance Evaluation Using ROC Curve

To provide a comparison to the RSFC maps derived from seed-based correlation, ICA, and the proposed ANN structure, the spatial patterns of all the estimated group maps were qualitatively compared based on the chosen golden standard. For more comprehensive evaluation, ROC curve was utilized in order to provide quantitative comparison. The selected golden standard is shown in Fig. 3.6. One of the fNIRS limitations is its low spatial resolution compared

Table 3.1. Number of neurons and activation function for each layers in the structure of ANN.

ANN Layer	No. of Neurons	Activation Function
Input layer	6667	ReLU
Hidden layer 1	1024	ReLU
Hidden layer 2	128	ReLU
Output layer	2	Softmax

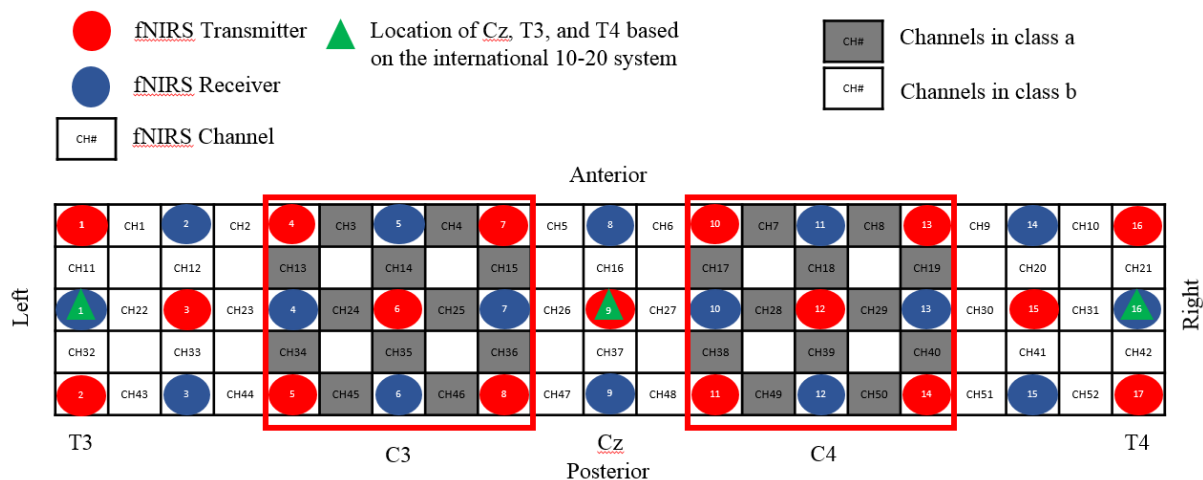


Figure 3.6. The selected golden standard for comparison evaluation in which the label of channels with gray and white background were set to 0 and 1, respectively.

to functional magnetic resonance (fMRI). Eventually, to localize the area corresponding Sensorimotor and Motor area, the channels which were approximately covering the C3 and C4 based on 10-20 system, were selected in one class (labeled as class (a)) versus the remained channels were set to the second class (labeled as class (b)) [13]. During the programing, the class (a) in golden standard for ANN were set to 0, however for seed-based and ICE analysis were set to 1. As ROC applies threshold values between 0 and 1, all the group RSFC results from aforementioned methods were normalized to the range of 0 to 1 by

$$val_i = \frac{val_i - \text{minimum}(val_1, \dots, val_{52})}{\text{maximum}(val_1, \dots, val_{52}) - \text{minimum}(val_1, \dots, val_{52})}, \quad (3.2)$$

where val_i is a result of the RSFC estimation method for the channel i . By utilizing ROC, it can be possible to digitize the real values of the estimated RSFC results. In ROC, the threshold value is a real number between 0 and 1 in which if the result value of a channel from the RSFC estimation method is higher than the threshold, then it is set to 1, vice versa, if it is less than the threshold, it is set to 0. After digitizing the real values, ROC curve can be derived by the *true-positive* and *false-positive* rates based on the golden standard labels.

IV. RESULTS

In the experiment, extracted resting-state oxygenated hemoglobin signals from the light intensities based on MBL method, were utilized to estimate resting-state functional connectivity maps by exploiting seed-based correlation analysis, independent component analysis, and artificial neural networks. In this chapter, the results of all aforementioned methods will be elaborated. Furthermore, the performance evaluation method based on receiver operating characteristic (ROC) curve will provide a comparison among all the obtained results.

For better comprehensive visualization of the filtered oxy-hemoglobin fluctuations during the resting-state, Fig. 4.1 shows the time series of the channel 24 and 29 versus 11 and 52 for one subject. The selected channels for visualization is based on their location in the configuration of fNIRS transmitters and receivers in which channels 24 and 29 cover the bilateral Sensorimotor, whereas channels 11 and 29 cover the Temporal areas. It is obvious that channels 24 and 25 has similar fluctuations. Same phenomenon happens for channels 11 and 21.

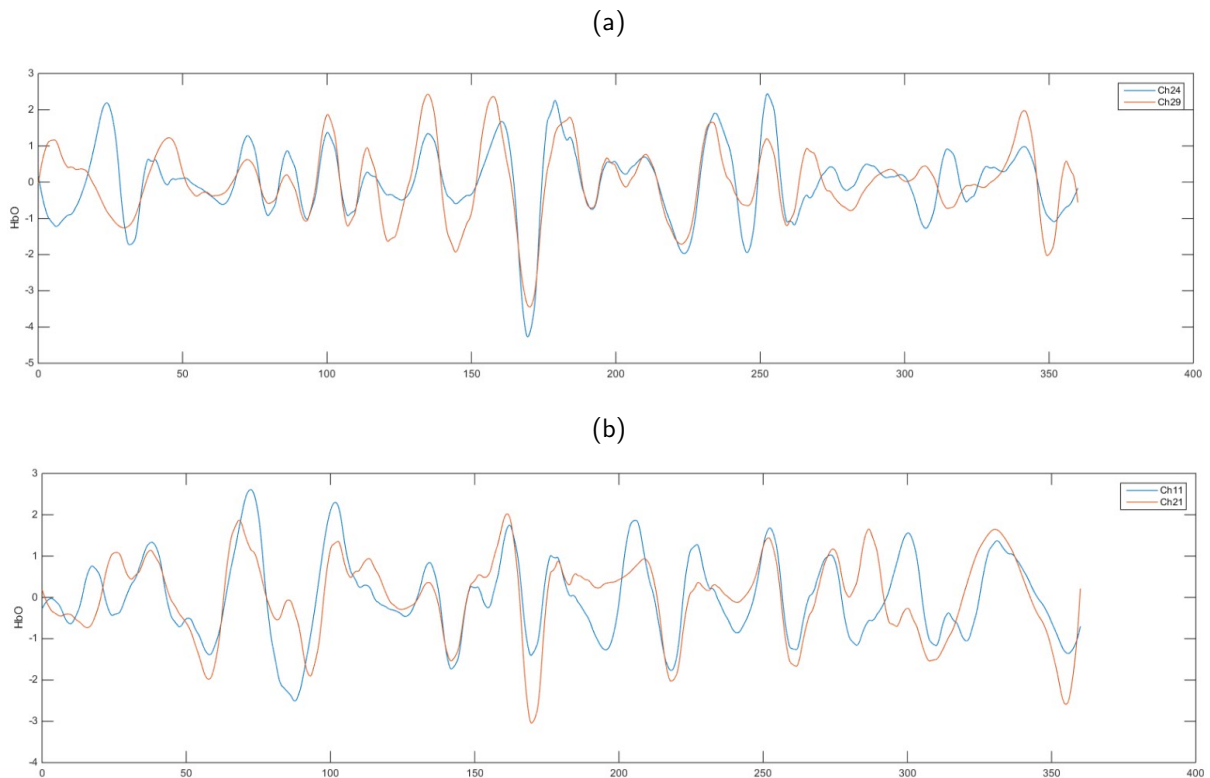


Figure 4.1. Oxy-hemoglobin of (a) channels 24, 29 and (b) channels 11, 52 for one subject.

The aim of all aforementioned methods is to detect similarity among time series fluctuations, though there is no pair of channels that fluctuate exactly the same.

1. Seed-based Correlation RSFC Results

From the Wilcoxon Signed-Rank group analysis on the individuals' GLM T -values of the task session, channel 24 (with lower p -value) showed the most significant activation based on the finger tapping task. Figure 4.2(a) shows the group activation map which was derived from implementation of GLM on the task session data. Consequently, the RSFC map from resting-state session based on selected channel is shown in Fig. 4.2(b). In this figure, the range of the t -values obtained by the statistical t -test, indicates the level of connectivity with channel 24. Warm colors represent the channels who had significant connectivity with the Sensorimotor seed.

For better visualization of the RSFC map, the empty spaces surrounded by channels were set to the mean value of the surrounding values (e.g. the space among channel 12, 24, 25,

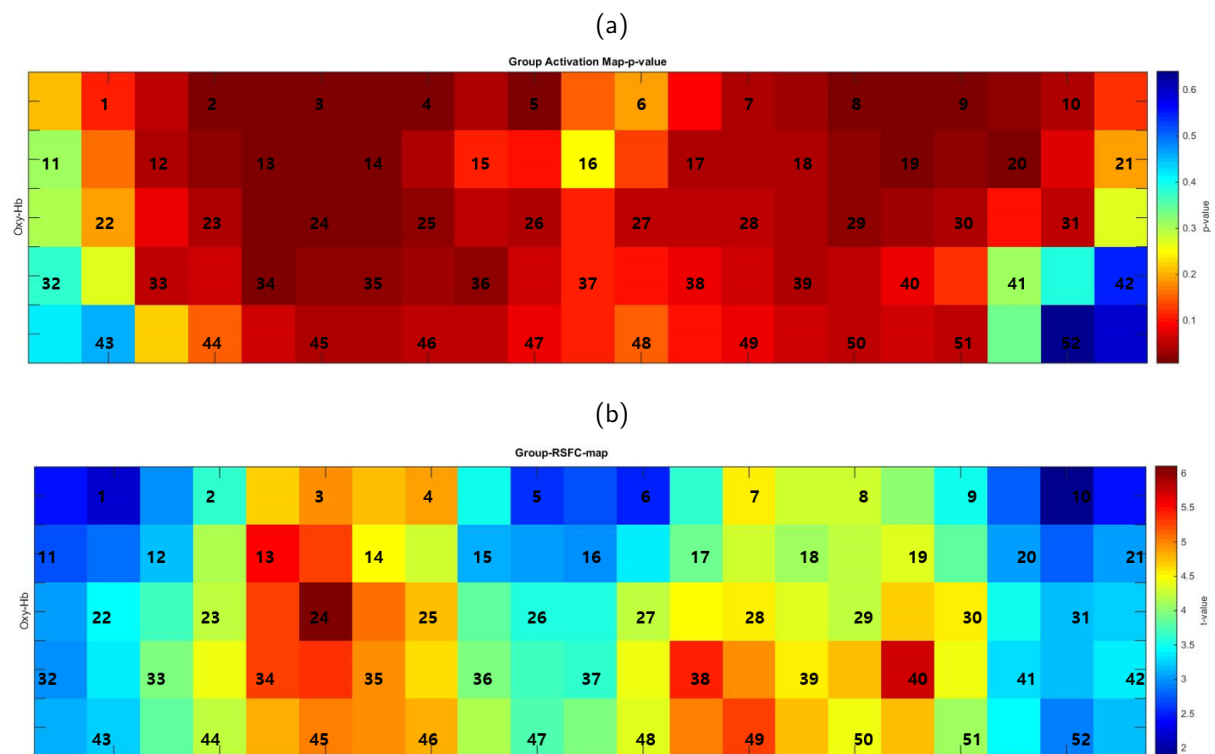


Figure 4.2. (a) Group activation map derived from task session using GLM. The lower p -value shows higher activation. (b) Group RSFC map derived from resting-state session based on the selected seed (i.e. channel 24) using GLM. The higher t -value shows higher connectivity with the seed.

and 35 is equal to the mean of them). In general, the RSFC pattern derived from seed-based correlation analysis using GLM, demonstrates similar pattern as expected based on the golden standard presented in Fig. 3.6. To be more specific, channels which are inside of the red square as the desire Sensorimotor region of interest (ROI) of Fig. 3.6 have significant correlation with the seed ($p < 0.0005$, critical t -value = 3.291).

2. ICA RSFC Results

As discussed in chapter II section 4., for each participant's resting-state time series the component of interest was selected based on its power spectrum.

Figure 4.3 illustrates two examples of the power spectrum derived from two independent components (IC). The red square in Fig. 4.3(a) demonstrates the desired range of frequency in which hemodynamic response fluctuates. Eventually, the RSFC corresponding to the IC1, the first column of the mixing matrix (i.e. \hat{A}) in this case, is shown in Fig. 4.3(c). Consequently, the group t -test analysis result from individual's ICA RSFC analysis can be found in Fig. 4.3(d). Same as the results derived from seed-based correlation analysis, the channels which are inside of the desire Sensorimotor ROI of Fig. 3.6 present more significant connectivity ($p < 0.001$, critical t -value = 3.091) compared to other channels covering Temporal areas of the brain.

3. ANN RSFC Results

In this section, the connectivity pattern based on training artificial neural network is presented. The time points of the filtered oxy-hemoglobin signals were used as the input layer for the proposed structure of the artificial neural network. Figure 4.4 represents the group level connectivity pattern derived from the proposed ANN structure. As discussed in section 5. of chapter II, the neural network was trained for 20 trials. Therefore, the output result for each channel was a value between 0 and 20 which represents the number of times that a specific channel was labeled for class (b). In Fig. 3.6, class (b) includes the channels outside of the desire Sensorimotor ROI (i.e. the area excluding Sensorimotor area). Afterwards, for better comprehensive comparison with the golden standard, the results were normalized to the range of 0 and 1 as shown in Fig. 4.4. In this figure, the channels with warmer color were labeled as

class (b) more frequently, whereas the channels with colder color were mostly set to class (a) during the testing procedure.

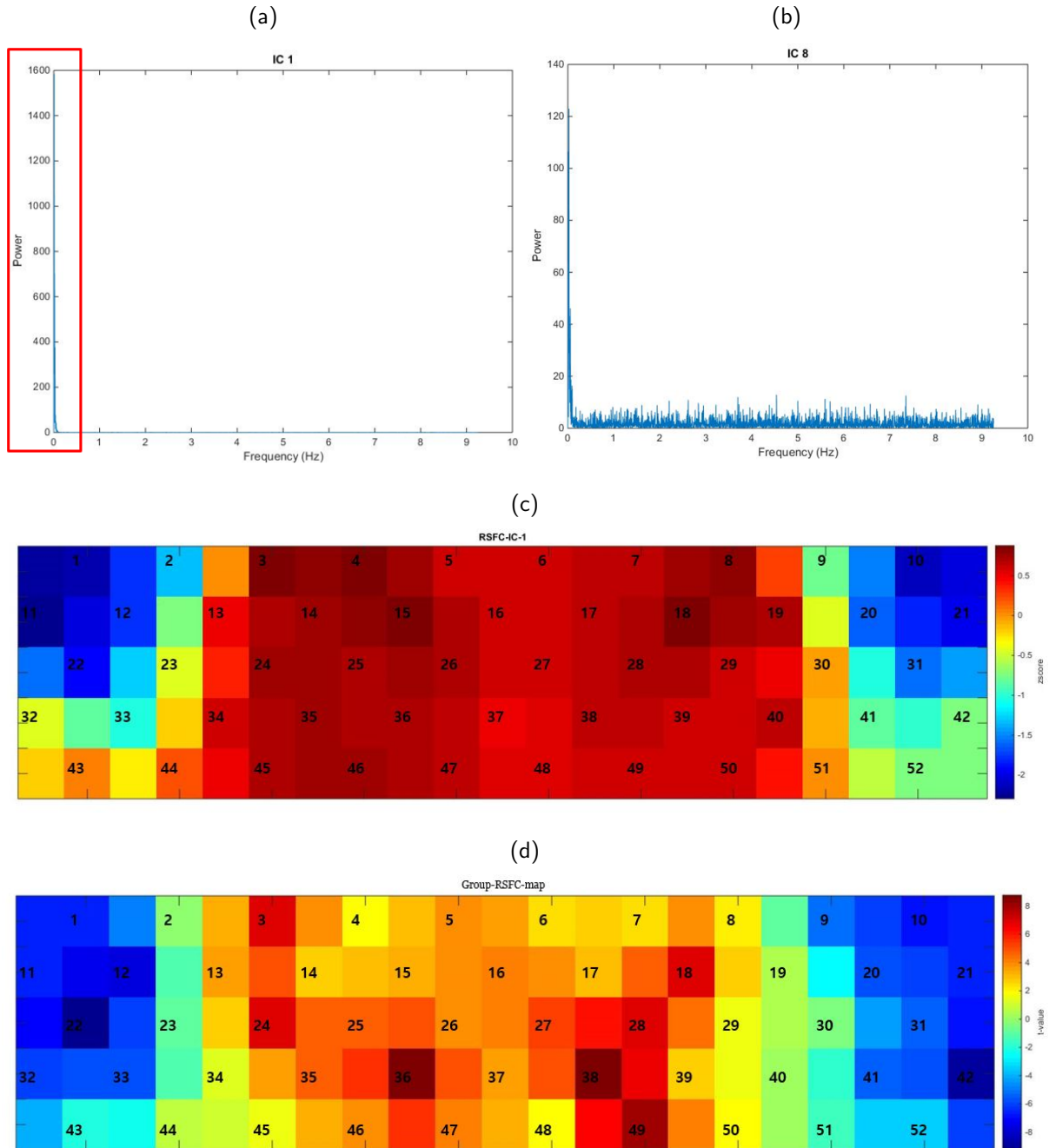


Figure 4.3. An example of the power spectra of (a) 1st and (b) 8th independent component derived from ICA analysis of one subject. (c) The corresponding RSFC map of IC1. (d) Group RSFC map derived from resting-state session using ICA.

4. ROC Evaluation Results

To provide a comparison to the group results from all the above mentioned methods, ROC curve is presented in Fig. 4.5. The group results were normalized to the range of 0 and 1 and their similarity with the golden standard was determined by ROC. In the golden standard for seed-based and ICA analysis the channels inside of the desire Sensorimotor ROI were labeled as class 1, whereas for ANN analysis, they were labeled as class 0. As in this thesis the aim is only finding two classes (or clusters), the labels were selected only in order to distinguish the classes.

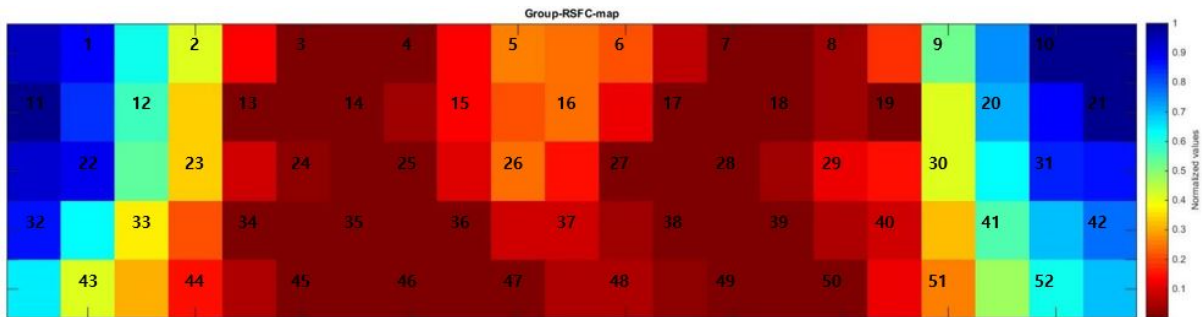


Figure 4.4. Group RSFC map derived from resting-state session using ANN.

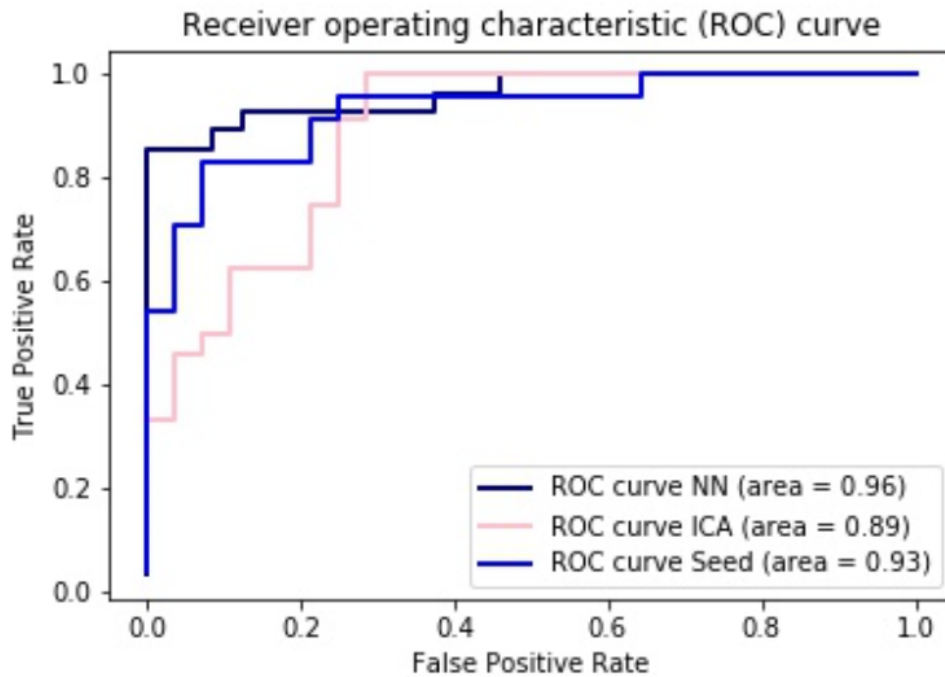


Figure 4.5. ROC curve. The area under the ROC curve of each method demonstrates their similarity to the golden standard.

The area under the ROC curve (AUC) illustrates a quantitative value of the similarity of the resting-state functional connectivity results with the golden standard. The AUC for seed-based analysis, ICA, and ANN are 0.93, 0.89, 0.96, respectively. Based on AUC performance evaluation, the proposed method for estimating functional connectivity based on artificial neural networks showed relatively better performance compared to the conventional methods.

V. Discussion and Conclusion

An accumulating body of evidence from previous studies suggest that resting-state functional connectivity is an important tool for exploration of brain diseases. The advances of several progressive methodologies in detecting RSFC patterns have been mentioned in previous studies. In this study, a new methodology based on artificial neural network was presented and its performance was compared with two widely used methods in RSFC studies.

Inspired by human brain system and regarding to the capabilities of artificial neural networks in system identification, this study focused on the feasibility of artificial neural network for resting-state functional connectivity detection. The spatial maps derived from the two conventional methods as well as proposed ANN-based method followed the connectivity patterns of the Sensorimotor area which were obtained in previous studies [8, 9, 13]. Eventually, the results highlighted the successful detection of RSFC by artificial neural networks.

ANN yielded slightly better performance in detection of the RSFC maps compared to the conventional methods. One important reason of the better performance of ANN in RSFC detection is that ANN can learn the behavior of a signal through its time points and set the learning weight values based on the difference of the values in each time point. Collectively, ANN was proposed as a promising approach in resting-state functional connectivity analysis. However, in order to train the network, two classes were chosen manually. Recent machine learning approach known as semi-supervised learning will be considered for choosing the classes automatically.

In seed-based analysis, as previously was reported, the results basically depend on the selection of the seed. However, in some studies the connectivity between specific ROI and non-ROI regions is the aim of the study in which seed-based analysis can be a suitable approach [8]. On the other hand, ICA-based analysis showed more localized connectivity patterns in previous studies [13], however, caution is needed in visually detection of the component of interest.

To date, it is not known which method is the most suitable approach in connectivity detection [8]. Despite all the above mentioned metrics, it should be noted that future investigations

should be taken into the consideration to understand the connectivity maps in both resting-state and task-based experiments including other brain regions as well.

References

- [1] O. Sporns, “Network attributes for segregation and integration in the human brain,” *Current opinion in neurobiology*, vol. 23, no. 2, pp. 162–171, 2013.
- [2] A. R. Carter, S. V. Astafiev, C. E. Lang, L. T. Connor, J. Rengachary, M. J. Strube, D. L. Pope, G. L. Shulman, and M. Corbetta, “Resting interhemispheric functional magnetic resonance imaging connectivity predicts performance after stroke,” *Annals of neurology*, vol. 67, no. 3, pp. 365–375, 2010.
- [3] A. G. Garrity, G. D. Pearlson, K. McKiernan, D. Lloyd, K. A. Kiehl, and V. D. Calhoun, “Aberrant ”default mode” functional connectivity in schizophrenia,” *American journal of psychiatry*, vol. 164, no. 3, pp. 450–457, 2007.
- [4] M. J. Lowe, M. D. Phillips, J. T. Lurito, D. Mattson, M. Dzemidzic, and V. P. Mathews, “Multiple sclerosis: low-frequency temporal blood oxygen level–dependent fluctuations indicate reduced functional connectivity—initial results,” *Radiology*, vol. 224, no. 1, pp. 184–192, 2002.
- [5] M. Assaf, K. Jagannathan, V. D. Calhoun, L. Miller, M. C. Stevens, R. Sahl, J. G. O’boyle, R. T. Schultz, and G. D. Pearlson, “Abnormal functional connectivity of default mode subnetworks in autism spectrum disorder patients,” *Neuroimage*, vol. 53, no. 1, pp. 247–256, 2010.
- [6] H. Zhu, J. Xu, J. Li, H. Peng, T. Cai, X. Li, S. Wu, W. Cao, and S. He, “Decreased functional connectivity and disrupted neural network in the prefrontal cortex of affective disorders: A resting-state fnirs study,” *Journal of Affective Disorders*, vol. 221, pp. 132–144, 2017.
- [7] N. Eshel, J. Huemer, L. McTeague, M. Wong, A. Yee, B. Patenaude, C. de los Angeles, and A. Etkin, “639-effect of rtms on resting-state functional connectivity in patients with major depression,” *Biological Psychiatry*, vol. 81, no. 10, p. S259, 2017.

- [8] H. Niu and Y. He, “Resting-state functional brain connectivity: lessons from functional near-infrared spectroscopy,” *The Neuroscientist*, vol. 20, no. 2, pp. 173–188, 2014.
- [9] C.-M. Lu, Y.-J. Zhang, B. B. Biswal, Y.-F. Zang, D.-L. Peng, and C.-Z. Zhu, “Use of fnirs to assess resting state functional connectivity,” *Journal of neuroscience methods*, vol. 186, no. 2, pp. 242–249, 2010.
- [10] J. San Juan, X.-S. Hu, M. Issa, S. Bisconti, I. Kovelman, P. Kileny, and G. Basura, “Tinnitus alters resting state functional connectivity (rsfc) in human auditory and non-auditory brain regions as measured by functional near-infrared spectroscopy (fnirs),” *PLoS One*, vol. 12, no. 6, p. e0179150, 2017.
- [11] F. Scholkmann, S. Kleiser, A. J. Metz, R. Zimmermann, J. M. Pavia, U. Wolf, and M. Wolf, “A review on continuous wave functional near-infrared spectroscopy and imaging instrumentation and methodology,” *Neuroimage*, vol. 85, pp. 6–27, 2014.
- [12] H. Liang, J. D. Bronzino, and D. R. Peterson, *Biosignal processing: Principles and practices*. CRC Press, 2012.
- [13] H. Zhang, Y.-J. Zhang, C.-M. Lu, S.-Y. Ma, Y.-F. Zang, and C.-Z. Zhu, “Functional connectivity as revealed by independent component analysis of resting-state fnirs measurements,” *Neuroimage*, vol. 51, no. 3, pp. 1150–1161, 2010.
- [14] M. J. McKeown, T. J. Sejnowski, *et al.*, “Independent component analysis of fmri data: examining the assumptions,” *Human brain mapping*, vol. 6, no. 5-6, pp. 368–372, 1998.
- [15] M. J. McKeown, S. Makeig, G. G. Brown, T.-P. Jung, S. S. Kindermann, A. J. Bell, and T. J. Sejnowski, “Analysis of fmri data by blind separation into independent spatial components,” tech. rep., NAVAL HEALTH RESEARCH CENTER SAN DIEGO CA, 1997.
- [16] G. Hinton, L. Deng, D. Yu, G. E. Dahl, A.-r. Mohamed, N. Jaitly, A. Senior, V. Vanhoucke, P. Nguyen, T. N. Sainath, *et al.*, “Deep neural networks for acoustic modeling in speech recognition: The shared views of four research groups,” *IEEE Signal Processing Magazine*, vol. 29, no. 6, pp. 82–97, 2012.

- [17] M. Anthony and P. L. Bartlett, “Neural network learning: Theoretical foundations,” 2009.
- [18] Y. A. LeCun, L. Bottou, G. B. Orr, and K.-R. Müller, “Efficient backprop,” in *Neural networks: Tricks of the trade*, pp. 9–48, Springer, 2012.
- [19] N. Talebi, A. M. Nasrabadi, and I. Mohammad-Rezazadeh, “Estimation of effective connectivity using multi-layer perceptron artificial neural network,” *Cognitive Neurodynamics*, pp. 1–22, 2017.
- [20] H. Liang, J. D. Bronzino, and D. R. Peterson, *Biosignal processing: Principles and practices*. CRC Press, 2012.
- [21] L. Chun-Lin, “A tutorial of the wavelet transform,” *NTUET, Taiwan*, 2010.
- [22] H. Tsunashima, K. Yanagisawa, and M. Iwadata, *Measurement of Brain Function Using Near-Infrared Spectroscopy (NIRS)*. INTECH Open Access Publisher, 2012.
- [23] S. Tak and J. C. Ye, “Statistical analysis of fnirs data: a comprehensive review,” *Neuroimage*, vol. 85, pp. 72–91, 2014.
- [24] T. J. Huppert, “Commentary on the statistical properties of noise and its implication on general linear models in functional near-infrared spectroscopy,” *Neurophotonics*, vol. 3, no. 1, pp. 010401–010401, 2016.
- [25] A. Hyvarinen and G. R. Naik, *Independent component analysis for audio and biosignal applications*. InTech, 2012.
- [26] M. Tkáč and R. Verner, “Artificial neural networks in business: Two decades of research,” *Applied Soft Computing*, vol. 38, pp. 788–804, 2016.
- [27] S. Raith, E. P. Vogel, N. Anees, C. Keul, J.-F. Güth, D. Edelhoff, and H. Fischer, “Artificial neural networks as a powerful numerical tool to classify specific features of a tooth based on 3d scan data,” *Computers in biology and medicine*, vol. 80, pp. 65–76, 2017.
- [28] V. Nair and G. E. Hinton, “Rectified linear units improve restricted boltzmann machines,” in *Proceedings of the 27th international conference on machine learning (ICML-10)*, pp. 807–814, 2010.

- [29] C. M. Bishop, *Pattern recognition and machine learning*. Springer, 2006.
- [30] D. Kingma and J. Ba, “Adam: A method for stochastic optimization,” *arXiv preprint arXiv:1412.6980*, 2014.
- [31] J. A. Hanley and B. J. McNeil, “The meaning and use of the area under a receiver operating characteristic (roc) curve.,” *Radiology*, vol. 143, no. 1, pp. 29–36, 1982.
- [32] Y. Gu, S. Miao, J. Han, K. Zeng, G. Ouyang, J. Yang, and X. Li, “Complexity analysis of fnirs signals in adhd children during working memory task,” *Scientific Reports*, vol. 7, 2017.
- [33] M. Okamoto, M. Matsunami, H. Dan, T. Kohata, K. Kohyama, and I. Dan, “Prefrontal activity during taste encoding: an fnirs study,” *Neuroimage*, vol. 31, pp. 796–806, 2006.
- [34] A. Hyvärinen and E. Oja, “Independent component analysis: algorithms and applications,” *Neural Networks*, vol. 13, no. 4, pp. 411–430, 2000.
- [35] H. Obrig, M. Neufang, R. Wenzel, M. Kohl, J. Steinbrink, K. Einhäupl, and A. Villringer, “Spontaneous low frequency oscillations of cerebral hemodynamics and metabolism in human adults,” *Neuroimage*, vol. 12, no. 6, pp. 623–639, 2000.

Acknowledgments

Apart from efforts, the success of this study depended mainly on the encouragement and guidelines of many others. First of all, I would like to express my sincere appreciation to my principle supervisor, Prof. Ji-Woong Choi and my co-supervisor, Prof. Hyeon-Ae Jeon for their valuable guidance and encouragement. I am truly grateful for their support and endless advices. This work would not have been possible without their assistance. I would also like to thank the committee member, Prof. Jae-Youn Hwang for his constructive comments and suggestions. I would like to appreciate all my lab members in CSP lab especially BMI group including Sung-Ho Lim, Kyungsoo Kim, Seongtak Kang, and Jin-Woo Yu for their precious help and supports throughout my time in DGIST.

To all my friends in DGIST, especially to Fatemeh Razmjooei who always supports me like my older sister and I will owe her forever, to Miguel Andres Luna whose constant help and valuable knowledge made the completion of this thesis possible, to Arup K George whose constant support helped me enormously in my life, to Akino Harauche for her moral supports in the ups and downs of my life in DGIST, and to Thanawin Trakoolwilaiwan whose kind help is very valuable in my life.

To all my Iranian friends who are not in Korea but their encouragements and warm supports made my stay in Korea more enjoyable. To Hanie Moghaddasi who taught me how does having a sister feel like, to Narges Nourian who taught me how a human can be ambitious in making the impossible possible, though her lost will never let me forget how she made me feel, to Mitra Ebrahimpoor who I owe her forever for her endless supports and valuable knowledge.

Last but not least, I am deeply grateful to my beloved family: my father Hamzeh-Ali Behboodi, my mother Tahereh Abbasi, my older brother Behrang Behboodi and his wife Sepide Kazemi. Although, they have not been literally beside me when I am finishing this manuscript, I would like to take this opportunity to mention that my family is all my inspiration and motivation for everything. I would like to appreciate them for all their supports and for allowing me to follow my ambitious. I will owe them forever for their endless kindness and love.

Curriculum Vitae

Name : Bahareh Behboodi
Date of Birth : June 22, 1991
E-mail : behboodibahareh@gmail.com, baharehb@dgist.ac.kr

Educations

2016. 03. – 2018. 02. M.S. Information and Communication Engineering ,Daegu Gyeongbuk Institute of Science & Technology (DGIST), Daegu, South Korea
2009. 09. – 2013. 09. B.S. Biomedical Engineering, Amirkabir University of Technology, Tehran, Iran

Professional Activities

2014. 05. – 2015.11. Research Assistant, Neuroimaging and Analysis Group (NIAG), Tehran, Iran

Publications

1. T. Trakoolwilaiwan, **B. Behboodi**, J. Lee, K. Kim, and J.-W. Choi, “Convolutional neural network for high-accuracy functional near-infrared spectroscopy in a brain-computer interface: three-class classification of rest, right and left hand motor execution”, *Neurophotonics*, 2017, 5(1)
2. T. Trakoolwilaiwan, **B. Behboodi**, and J.-W. Choi, “Convolutional Neural Network for Functional Near-Infrared Spectroscopy in Brain-Computer Interface,” Winter Conference, *Korea Information and Communications Society (KICS)*, (한국통신학회 동계학술대회), Jan 2017.
3. **B. Behboodi**, K. Kim, and J.-W. Choi, “Eye Blinks Motion Artifact Removal Using Kurtosis-based Wavelet Algorithm in Prefrontal Area”, fNIRS2016 Conference, *Paris, France*, Oct. 2016